Indian Journal of Chemical Technology
Vol. 25, May 2018, pp. 287-293

Kinetic study of the dissolution of metakaolin with hydrofluoric acid

Eliana G Pinna[1,2], Lucía I Barbosa[2], Daniela S Suarez[1] & Mario H Rodriguez*[,1]

[1]Laboratorio de Metalurgia Extractiva y Síntesis de Materiales (MESiMat), FCEN-UNCuyo-CONICET, Padre Contreras 1300, CP 5500, Mendoza. Argentina.

[2]Instituto de Investigaciones en Tecnología Química (INTEQUI), UNSL-CONICET, Chacabuco y Pedernera, CP 5700, San Luis, Argentina.

E-mail: mrodriguez@uncu.edu.ar

Received 3 March 2016 ; accepted 17 April 2017

The kinetics mechanism on the dissolution of metakaolin by hydrofluoric acid has been studied. The effects of temperature, reaction time, and stirring speed have been examined. Experimental results show that reaction rate increases with both temperature and reaction time. The global process of metakaolin dissolution with HF is characterized with an apparent activation energy of 21.096 kcal/mol, which indicates that the reaction rate is mainly controlled by the chemical stage. Experimental data fitted the sequential nucleation and growth model.

Keywords: Kinetics, Modeling, Metakaolin, Dissolution, Aluminum, Silicon

Bauxite is the principal raw material for the commercial production of aluminum through the Bayer and Hall-Héroult processes. Although, the proved reserves of bauxite may supply the world aluminum industry only for a few centuries. Many investigators have sought processes using raw materials other than bauxite, such as clay and kaolinite[1]. These are materials containing from 10 to 20% w/w of aluminum. According to Altiokka *et al.*, the kaolinitic clay, abundant in nature, is an alternative raw material in the production of alumina.

Fogler *et al.*[3] reported a study on the dissolution of sodium and potassium feldspar in HF/HCl acid mixtures. They proposed that the dissolution is limited by the rate at which HF reacts with the solid surface and the strong influence of HCl on the dissolution rate is due to the adsorption of H^+ ions on the mineral surface. Kline and Fogler[4] researched the dissolution of silicate minerals, kaolin among them, in HF/HCl mixtures, concluding that the dissolution of these minerals by HF is a catalyzed system in which the rate of attack by molecular HF is increased by the presence of additional strong acids in the reacting mixture. It was agreed that overall dissolution consists of two parallel surface reactions: an uncatalyzed attack by adsorbed HF molecules and a reaction catalyzed by the presence of adsorbed protons. Kline and Fogler[5] studied the relation between the dissolution kinetics of silicates in HF and the chemical species present in solution. They concluded that dissolution rates can be attributed to the attack by the HF molecules adsorbed at the surface rather than by F^-or HF_2^-ions.

The calcination of kaolin aimed for the phase transformation into metakaolin increases the mineral reactivity since in the latter structure, aluminum is extremely susceptible to the acid attack[6-8].

The kinetics of the dissolution reaction of metakaolin has been studied using different leaching agents such as hydrochloric acid[9-10], sulfuric acid[9,11], and nitric acid[9]. The reported values of apparent activation energy correspond to a chemically controlled process. Furthermore, it is agreed that the dissolution kinetics follows the unreacted core model for spherical particles. To date, no studies on the kinetics of metakaolin dissolution in HF have been reported.

The aim of the present work is to study the kinetics and mechanism of the reaction between metakaolin and HF. Experimental data concerning the effect of different variables upon the system reactivity led to the proposal of a mechanism and a kinetic reaction model and a global understanding of the kaolinite dissolution process.

Experimental Section

Materials

The hydrofluoric acid used was brand Biopack, 40% v/v of analytical grade. The sample used in this study was kaolin obtained in the deposit Sur del Río, Argentina. The bulk composition of the ore is shown in Table 1, as determined by XRF.

With regard to particle size distribution, 69% of the sample is composed of particles smaller than 75 µm and the remaining 31% include particles ranging in size from 100 to 300 µm. The particle size selected for this study was -75µm.

Table 1 — Bulk composition of the mineral.

Component	SiO_2	Al_2O_3	Fe_2O_3	TiO_2	K_2O	Na_2O	CaO	MgO	Other
% w/w	65.20	22.30	1.07	0.27	0.51	0.28CaO	0.66	0.21	9.50

Equipment

Characterization of reactants and products was performed by X-ray fluorescence (XRF) on a Philips PW 1400 instrument and by X-ray diffraction (XRD) in a Rigaku D-Max III C diffractometer, operated at 35 kV and 30 mA. Morphological analysis was done by scanning electron microscope (SEM) in a LEO 1450 VP instrument which was equipped with an X-ray dispersive spectrometer EDAX, Genesis 2000. The metallization of the samples was performed with Au. Analysis of the specific area was carried out by BET method using a Micromeritis Gemini V equipment.

Characterization of the sample

The kaolin sample was calcined from room temperature to 1173 K in N_2 atmosphere at a heating rate of 10 K/min in order to transform it into metakaolin phase, which is more susceptible to the acid dissolution. The calcination assay was performed in a thermogravimetric system designed in our laboratory[12]. The thermogravimetric curve obtained shows two mass loss zones (Fig. 1).

The first zone exhibits a mass loss of 2% and corresponds to the removal of physically adsorbed water on the kaolin surface. The second region corresponds to kaolinite dehydroxylation, according to reaction (1):

$$Al_2Si_2O_5(OH)_{4(s)} \rightarrow Al_2O_3 2SiO_{2(s)} + 2H_2O_{(g)} \quad ...(1)$$

Figure 1 shows that the transformation of kaolinite into metakaolinite is complete at 1073 K.

The ore sample was analyzed by XRD before and after the thermal treatment and the results are shown in Figs. 2 a) and 2 b), respectively. The phases identified in the diffraction pattern shown in Fig. 2 a) are kaolinite (ICDD 01-089-6538), quartz (JCPDS 33-1161), and pyrophyllite (JCPDS 012-0203); the two latter are present in the ore as gangue. The diffraction pattern of the calcined ore shows only the presence of the gangue since metakaolin is a non-crystalline solid.

The morphology analysis of kaolin and metakaolin particles is presented in Figs. 2 c) and 2 d), respectively. Both samples present particles with laminar structure, thus after dehydroxylation, some degree of organization (structural and morphological) is still present.

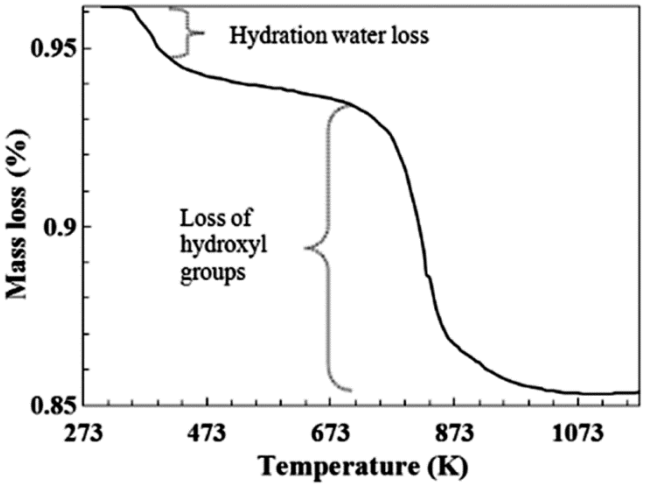

Fig. 1 — Thermogram corresponding to the kaolin sample calcined between room temperature and 1073 K.

Kaolinite mineral is composed by tetrahedral (SiO_4) and octahedral (AlO_6) sheets. These sheets form elemental clusters based on the tetrahedral-octahedra combination. The combination among *n* elemental clusters through the hydrogen bond provided by OH^- ions of the octahedral sheet builds up the mineral structure. This structure exhibits an order along *a*, *b*, and *c* axes. During the process of transformation of kaolinite into metakaolinite by calcination, the hydrogen bond is broken followed by a process of dehydroxylation and a change in the co-ordination of aluminum from six to four. Order is maintained along the axes *a* and *b*, but disappears along the axis *c* (According to Gastuche et al.[13]); this alteration explains the greater reactivity of metakaolinite towards chemical reagents.

Experimental procedure

The leaching tests were performed in a closed batch reactor of 800 mL built in Teflon® and equipped with magnetic stirring and temperature control systems.

For each test, 10 g of metakaolin, obtained as described in the previous section, and 450 mL of distilled water were introduced into the reactor. This mixture was heated to attain the work temperature. Subsequently, 50 mL of HF was added and the reaction time began to be measured. At the end of this period, the solid was filtered, dried at 348 K, and weighed.

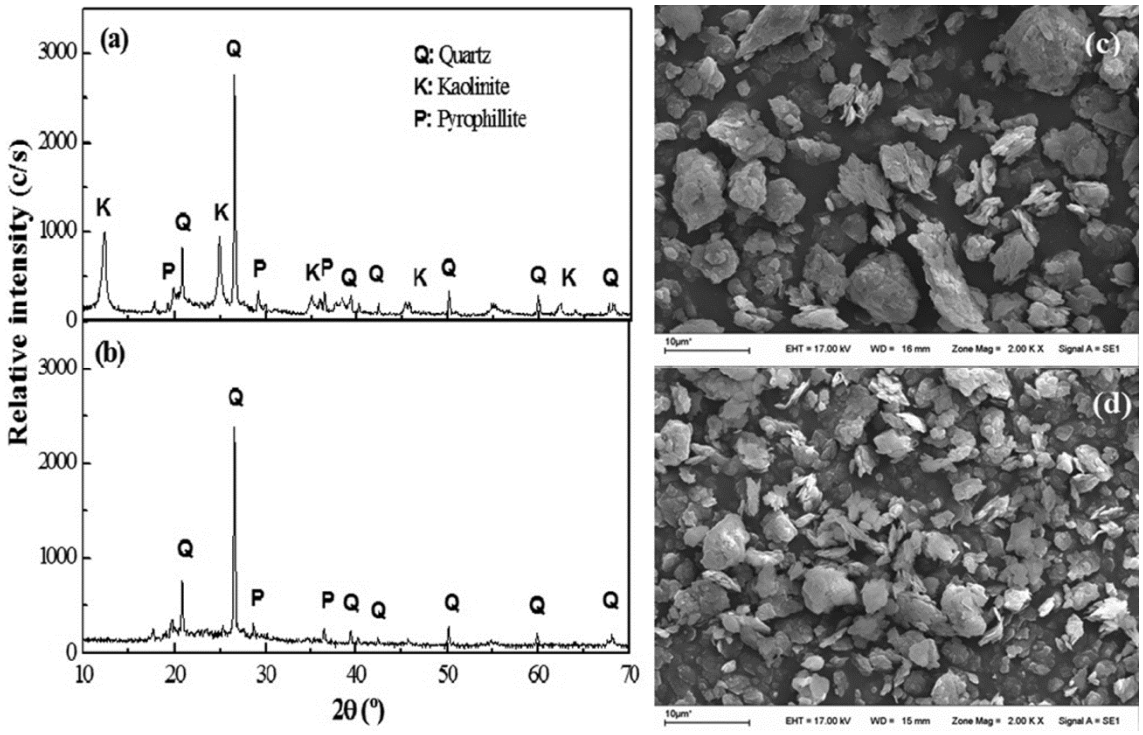

Fig. 2 — XRD patterns of a) kaolin sample and b) calcined kaolin. SEM micrographs: c) kaolin and d) metakaolin.

Results and Discussion

Based on the study by Rosales *et al.*[14], we propose that the dissolution of metakaolin in HF occurs as it follows:

$$Al_2O_3 2SiO_{2(s)} + 24HF_{(aq)} \rightarrow 2H_3AlF_{6(aq)} + 2H_2SiF_{6(aq)} + 7H_2O \quad ...(2)$$

The degree of dissolution of solid reactant X was calculated[15] as follows:

$$X = (m^o - m^f)/m^o \quad ...(3)$$

where: m^o is the initial mass of the mineral and m^f the mass of the mineral remaining unattacked by HF, which is subsequently filtered and dried. This equation is valid when the reaction of dissolution does not yield solid products. This condition is fulfilled in our reaction system since unreacted metakaolin mineral was the only compound found in the residual samples of each leaching experiment, as confirmed by XRD and SEM analysis.

Effect of the stirring speed

Leaching tests were carried out to evaluate the effect of the stirring speed on the dissolution of metakaolin from 110 to 550 rpm at 298 K for 30 min using 10% v/v HF with a solid-to-liquid ratio of 1/50 and particle size of 75 µm. The results presented in Fig. 3 a), show that the stirring speed does not have a remarkable effect on the dissolution rate. This indicates that the mass transfer rate in the solid-liquid interface is not involved in the global reaction rate of the process.

Effect of temperature and reaction time

Figure 3b. shows the effect of reaction time on the dissolution of the mineral at 278, 283, 288, and 318 K for periods from 0.5 to 20 min. The leaching tests were carried out under following conditions: solid-to-liquid ratio, 1/50; stirring speed, 330 rpm; particle size, 75 µm and HF concentration, 10% v/v. The results show that the dissolution rate of the mineral depends strongly on both temperature and reaction time.

Characterization of leaching residues

SEM micrographs of the residues of metakaolin leached for periods from 1 to 25 min are shown in Figs. 4 (a-d) For periods lower than 15 min, the residues particles exhibit small holes. For longer periods, the original small holes grow to a great extent.

Kinetic model and mechanism

The kinetic model was estimated running the software MODELADO using the experimental data obtained at different temperatures (Fig. 5). These data were correlated with 32 different models. The

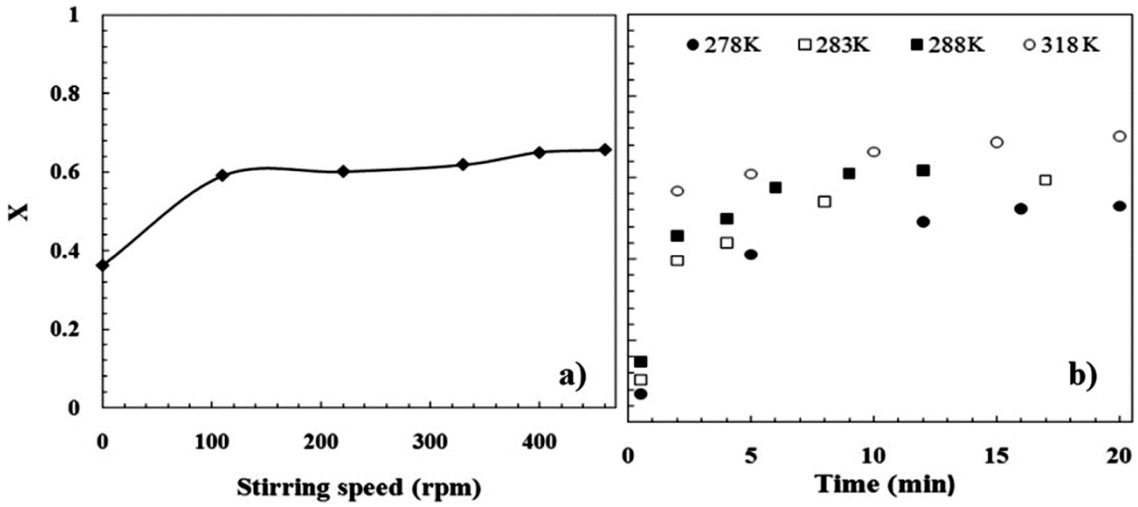

Fig. 3 — Effect of a) stirring speed and b) time on the dissolution rate.

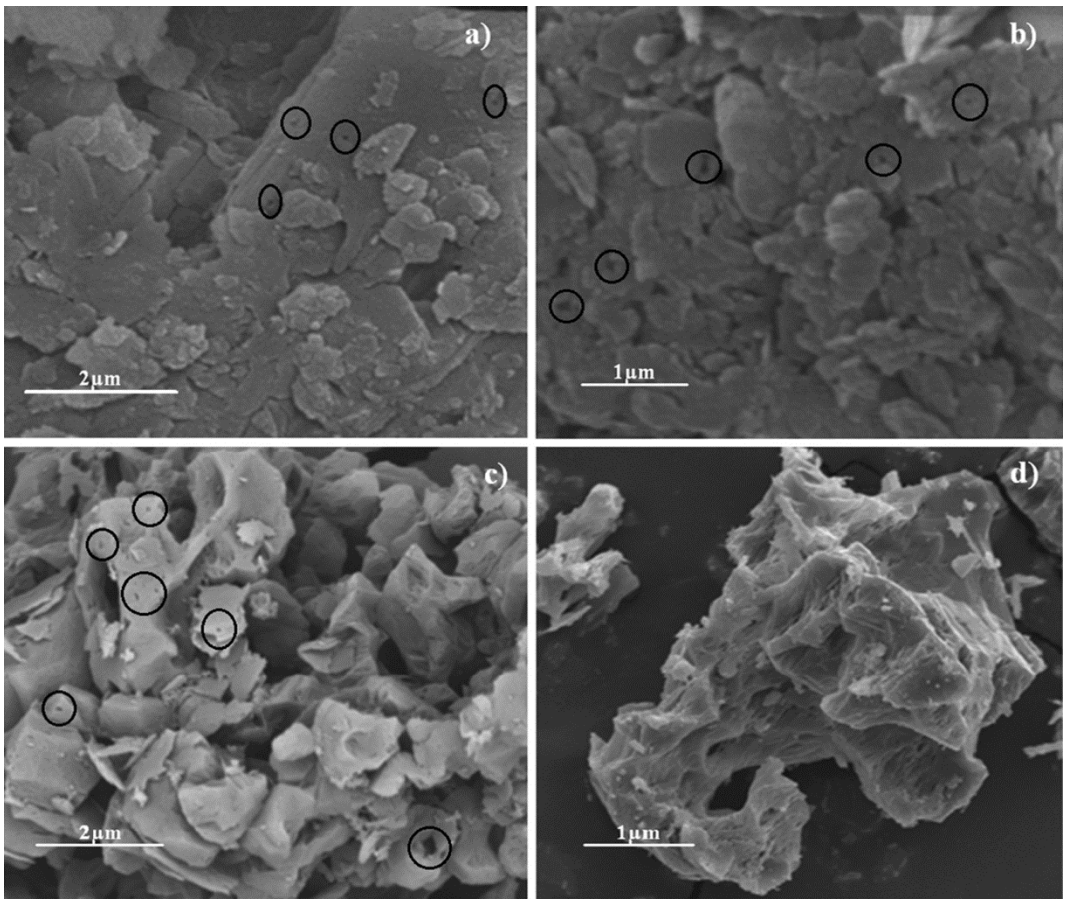

Fig. 4 — SEM micrographs of the residual samples leached for different periods: a) 1 min, b) 2 min, c) 10 min, and d) 25 min.

operation conditions used for each assay, were entered as a set of inputs to start the estimation. Where: T is the reaction temperature; m^o initial mass of the sample; d^o diameter of the particle or the least of its characteristic lengths; C_a concentration of HF; n_r stirring speed; ε error associated to each level of temperature.

Each model is classified according to assumptions regarding the reactant particle: its reactivity, starting structure, and changes underwent during the process

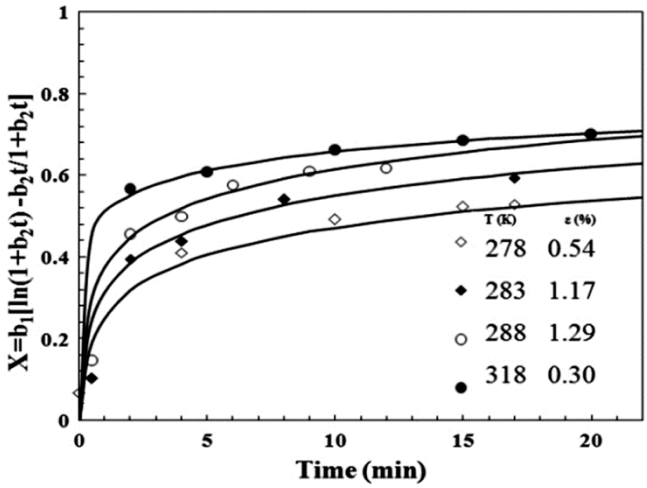

Fig. 5 — Mathematical fit of the experimental data of metakaolin dissolution in HF at different temperatures. Kinetic model (line); experimental data (symbol).

of transformation. Thus, such models are grouped into the following types of reactions:

Type I reactions: a) the particle is composed of a non-porous pure solid; b) there is no formation of solid products remaining on the particle; c) during the whole process, the interface surface is uniformly reactive and identical to the surface of the particle.

Type II: a) the interface surface is uniformly reactive; b) the process begins when the solid and fluid reactants are brought into contact; c) the reactant particle has initially or during the reaction one or more porous regions.

Type III: a) the particle is composed of a non-porous pure solid; b) there is no formation of solid products remaining on the particle; c) the interface surface is identical to the surface of the reactant particle; d) the initial reaction rate of the process is controlled by the rate of formation of the reaction interface. As regard the formation of the reaction interface, the following two cases should be distinguished: topochemical reactions and reactions that proceed by activation of the interface area.

Type IV: a) the initial reaction rate of the process is controlled by the rate of formation of the reaction interface; b) the reactant particle has initially or during the reaction one or more porous regions. These reactions can occur in six different cases, which are given by combining reactions type II and type III.

In addition, each formulated model has several particular hypotheses that make them differ from each other.

The sequential nucleation and growth model best fitted the experimental data of metakaolin dissolution in HF at different temperatures. The mathematical expression of this model is as follows:

$$X = b_1 [\ln (1 + b_2 t) - b_2 t / (1 + b_2 t)] \quad ...(4)$$

where b_1 and b_2 are correlation coefficients of the model. For the deduction of the proposed model, the number and rate of generation of spontaneous active sites were calculated. As regards this model, the generation of these sites in the metakaolin-HF reaction system is that of the "sequential" type (Quiroga *et al.*). In which case, the rate of change of the number of spontaneous active sites generated sequentially on the interfacial surface of the reactant particle is expressed in Eq. (5)[15].

$$r_N = dN_S/dt \quad ...(5)$$

where: N_S is the actual number of active sites per unit area of the reactant initial particle and r_N is the rate of generation of active sites per unit area of the initial surface on the reactant particle.

The generation of active sites occurs by nucleation of a chemical specie E, (HF in our case) which is adsorbed on the initial surface of metakaolin.

By introducing the order of nucleation β, a model for r_N can be obtained. Eq. (6) gives the expression of r_N for $\beta = 2$.

$$r_N = k_{N2} N_E^{\,2} / [1 + k_{N2} N_E^{\,0} (t - t_L)] \quad ...(6)$$

The approximate method given by Delmon[21] is used to analyze the kinetics of this type of transformations, which occur at constant r_s. First, vg is reformulated. Second, a relation between X and the total volume of germs is defined. Finally, this relation is combined with the equation given for r_N.

The volume occupied by an immaterial germ is calculated as a function of the dimensionless time τ according to the following equation.

$$v_g = \sigma_g V^o \tau^\lambda \quad ...(7)$$

$$\tau = b\, m_B r_s / \rho d^o)\, (t - t_L) \quad ...(8)$$

The degree of conversion X experienced by a reactant particle, on which several immaterial germs grow was calculated as a relation between the total volume of germs and the volume of the initial particle surface as follows:

$$X = V_G / V^o \quad ...(9)$$

In the case of sequential generation of active sites, the total volume of germs was calculated according to Eq. (10). The rate of change of the degree of conversion was calculated by combining Eq. (9) and (10), leading to Eq. (11).

Table 2 — Experimental conditions of metakaolin dissolution assays at different temperatures.

Run	T (K)	ε (%)	m^o (g)	d^o (μm)	C_a (v/v)	n_r (rpm)	b_1	b_2	$k = b_1 b_2$
1	278	0.54	10	75	0.10	460	0.0966	36.0	3.4776
2	283	1.17	10	75	0.10	460	0.103	56.7	5.8401
3	288	1.29	10	75	0.10	460	0.105	94.9	9.9645
4	318	0.30	10	75	0.10	460	0.0661	5730	378.753

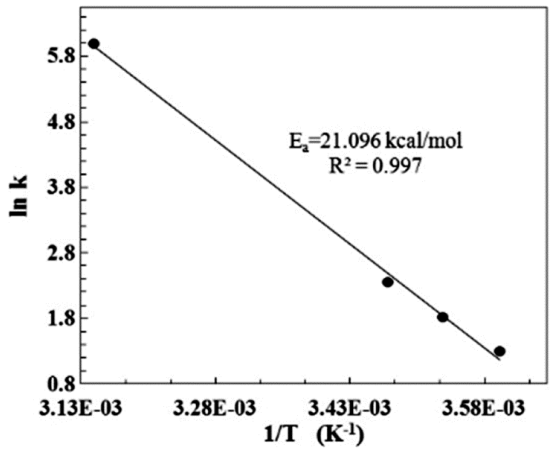

Fig. 6 — Arrhenius plot for the dissolution of metakaolin in HF.

$$V_G = \int_0^t \Omega^0 v_g r_N \, dt \quad ...(10)$$

$$dX/dt = (1/V^o)\, dV_G/dt = \Omega^0 v_g r_N / V^o \quad ...(11)$$

Equation (12) is obtained by combining Eq. (11) with Eq. (7) and (8), and considering that $dt = (\rho\, d^o / b\, m_B\, r_s)\, d\tau$. The replacement of r_N in Eq (12) by the expression from Eq. (6) gives Eq. (13).

$$dX/d\tau = (\sigma_g \Omega^0 \rho\, d^o r_N / b\, m_B r_S)\tau^\lambda \quad ...(12)$$

$$dX/d\tau = [\sigma_g \Omega^0 \rho\, d^o k_{N2} N^2{}_E{}^o / b\, m_B\, r_S\, [1 + k_{N2} N_E{}^0 (t-t_L)]^2]\tau^\lambda \quad ...(13)$$

The replacement of t-tL in Eq. (13) by Eq. (8) leads to Eq. (14):

$$dX/d\tau = \{\sigma_g\, \Omega^0\, \rho\, d^o k_{N2}\, N^2{}_E{}^o / b\, m_B\, r_S\, [1 + k_{N2} N_E{}^0 (\rho\, d^o \tau / b\, m_B\, r_S)]^2\}\tau^\lambda \quad ...(14)$$

If we define $b_1 = \sigma_g\, \Omega^0\, N_E{}^0$ and $b_2 = d^o\, k_{N2}\, N_E{}^0 / b\, m_B\, r_S$ and then these expressions are introduced in Eq. (14), we obtain Eq. (15).

$$dX/d\tau = [b_1\, b_2 / (1 + b_2\, \tau)^2]\, \tau^\lambda \quad ...(15)$$

Taking into account SEM results, the growth of active sites occurs in one direction, thus $\lambda = 1$.

The values of the kinetic parameters estimated by the software are shown in Table 2. The kinetic constant is defined as the product between b_1 and b_2.

The results of experimental data adjustment of the dissolution of metakaolin in HF with the model are shown in Fig. 5. The experimental results and the values predicted by the kinetic model are in excellent agreement, as can be seen from ε values (Table 2).

The activation energy was calculated from a plot of ln k versus 1/T and these results are presented in Fig. 6. According to Habashi[22], the estimated apparent activation energy value of 21.096 kcal/mol indicates that the chemical stage plays a very important role on the control of the reaction rate. Two stages could have been involved in the dissolution reaction: a slow stage that controls the reaction rate and a fast stage.

Stage 1 (slow): chemical adsorption of the reactive fluid

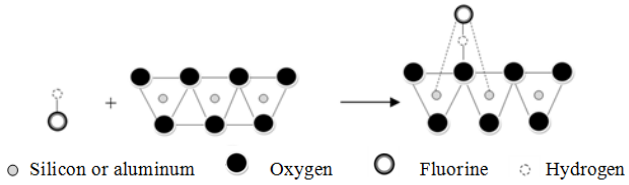

Stage 2 (fast): chemical desorption of the fluid product

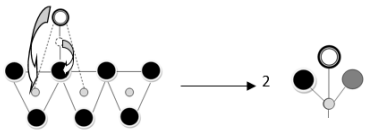

Overall reaction

$$Al_2O_3 2SiO_{2(s)} + 24HF_{(aq)} \longrightarrow 2H_3AlF_{6(aq)} + 2H_2SiF_{6(aq)} + 7H_2O \quad ...(2)$$

The chemical attack occurs through the chemical adsorption of the HF molecule on the surface of the mineral followed by the chemical reaction and the chemical desorption of the fluid products H_3AlF_6 and H_2SiF_6 as in the cases reported for kaolin. The breaking of the hydrogen bonds and the shrinkage of the c parameter induced both by the transformation of kaolin into metakaolin account for the accessibility of the interlayer surface to HF. The growth of the holes in one direction with the increase of time leads to the collapse of the laminar structure due to the growth of the nuclei. The causes of the origin of preferential sites of interaction can be diverse, such as heterogeneities, which often have solid surfaces,

caused by crystal defects or impurities in the solid[15,22]. In the case of metakaolin structure, the preferential sites of acid attack are mainly related to the contraction of the c parameter as a result of the calcined process.

Conclusions

The experimental results reveal that the increase of both temperature and time favours the metakaolin dissolution reaction, yielding conversions over 70% at 318 K. The increase of the stirring speed slightly affects the dissolution of mineral above 110 rpm. Furthermore, experimental data fitt the sequential nucleation and growth model with a nucleation of second order and a one-dimensional preferential nucleation. The value found for the apparent activation energy, 21.096 kcal/mol, indicates that the chemical stage plays a very important role on the control of the reaction rate.

Appendix

b	:	Stoichiometric coefficient.
C_a	:	Concentration of HF evaluated on the interface of reaction, mol/L.
d^o	:	Initial particle diameter, μm.
E_a	:	Activation energy, kcal/mol.
K	:	Kinetic coefficient of the reaction rate, m/s.
k_{N2}	:	Kinetic coefficient of the formation of the sites, m^2/s.
m_B	:	Molecular weight of the solid reactant, g/mol.
m^o	:	Initial mass of the mineral, g.
m^f	:	Mass of the mineral remaining unattacked, g.
N_E^0	:	Number of moles per unit area of a chemical specie E.
N_S^0	:	Initial number of the sites than can be activated per unit area of the initial surface of the reactant particle.
N_S	:	Number of active sites per unit area.
λ	:	Growth factor.
r_N	:	Activation sites rate, mol m^{-2} s^{-1}.
r_S	:	Solid-fluid reaction rate, mol m^{-2} s^{-1}.
T	:	Temperature, K.
t	:	Time, s.
t_L	:	Latency time, s.
τ	:	Dimension less time.
v_g	:	Volume of the hole, m^3.
V_G	:	Total volume of holes, m^3.
V^0	:	Initial particle volume, m^3.
X	:	Degree of dissolution of the solid reactant.
p	:	Solid density, kg/m^3.
Ω^0	:	Initial particle surface, m^2.
σ_g	:	Shape coefficient of holes.
β	:	Nucleation order.
ε	:	Error associated to each level of temperature.
n_r	:	Stirring speed, rpm.

References

1 Habashi F, *Handbook of Extractive Metallurgy*, (Wiley-VCH,Germany), 1997.
2 Avgustinik A I, *Cerámica* (Reverté, S A, Barcelona), 1983.
3 Fogler H S, Lund K & Mc Cune CC, *Chem Eng Sci*, 30, (1975), 1325.
4 Kline W E & Fogler H S, *J Colloid Interf Sci*, 82, (1980) 93.
5 Kline W E & Fogler H S, *Ind Eng Chem Fundam*, 20, (1981)155.
6 Gajam S Y & Raghavan S, *Hydrometallurgy*, 15, (1985) 43.
7 Colina F G & Costa J, *Ind Eng Chem*, Res.44, (2005) 4495.
8 Uzun D & Gulfen M, *Indian J Chem Technol*, 14 (2007) 263.
9 Hulbert S F & Huff D E, *Clay Miner*, 8, (1970) 337.
10 Altiokka M R, Akalin H, Melek N & Akyalçin S, *Ind Eng Chem Res*, 49, (2010) 12379.
11 Altiokka M R & Hoşgün H L, *Hydrometallurgy*, 68, (2003) 77.
12 Tunez F M, González J & Ruiz M C, Aparato de Laboratorio para Realizar Termogravimetrías en Atmosferas Corrosivas y no Corrosivas (in spanish), Argentina Patent, Appl P060100450, 2007.
13 Gastuche M C,Toussaint, F, Fripiat J J, Touilleaux R & Meersche M Van, *Clay Miner*, 5, (1963) 227.
14 Rosales G D, Ruiz M C & Rodriguez M H, *Hydrometallurgy*, 139, (2013) 73.
15 Quiroga O D, Avanza, J R & Fusco A J, *Modelado Cinético de las Transformaciones Fluido-Sólido Reactivo* (EUDENE, Corrientes), 1996.
16 Rosales G D, Ruiz M C & Rodriguez M H, *Minerals*, 98, (2016) 6.
17 Pinna E G, Ruiz M C, Ojeda M W & Rodriguez M H, *Hydrometalurgy*, 167, (2017) 66.
18 Quiroga O D & *MODELADO. Software para el tratamiento cinético de las transformaciones fluido-Sólido Reactivo.* (INIQUI UNSa-CONICET, Corrientes), 2000.
19 Rodriguez M H, Quiroga O D & Ruiz M C, *Hydrometallurgy*, 85, (2007) 87.
20 Barbosa L I, Valente N G & González J A, *Thermochim Acta*, 557, (2013) 61.
21 Delmon B, *Introduction a la cinétique hétérogène* (technip, Paris), 1969.
22 Habashi F, *Extractive Metallurgy General Principles* (Gordon and Breach Science Publishers, New York), 1980.